Available online at www.sciencedirect.com
ScienceDirect
Sensors and Actuators A 132 (2006) 245–251
SENSORS AND ACTUATORS A PHYSICAL
www.elsevier.com/locate/sna

Effects of the elastic cover on tactile sensor arrays

Gábor Vásárhelyi [b,*], Mária Ádám [a], Éva Vázsonyi [a], István Bársony [a], Csaba Dücső [a]

[a] *Research Institute for Technical Physics and Materials Science (MFA), Hungarian Academy of Sciences, P.O. Box 49, H-1525 Budapest, Hungary*
[b] *Péter Pázmány Catholic University, Department of Information Technology, Práter utca 50/a, H-1083 Budapest, Hungary*

Received 9 September 2005; received in revised form 5 December 2005; accepted 13 January 2006
Available online 20 February 2006

Abstract

Tactile sensors are composed of two substantial parts, the sensory structure and its cover. The characteristics of a sensor are fundamentally set by the sensor design, but are also essentially modified by the elastic cover on top. In this paper we analyze the pure mechanical information-coding effects of the sheltering rubber layer, applied on single-crystalline silicon 3D-force sensors, capable to detect both normal and shear forces. We give instructions on how to enhance the sensor's sensitivity by mimicking human tactile perception with introducing hair- and fingerprint-like elements to the sensor design.

Keywords: Tactile sensor; Elastic cover; Semi-infinite elastic model; Receptive field

1. Introduction

Artificial tactile sensors are simple models of the peripheral part of human touch. Sensors are analogues of the mechanoreceptors while the protective coating is similar to the skin. Besides protecting the sensors from damage, this elastic medium acts as an information-coding layer, and thereby plays a crucial role in determining the sensor's characteristics.

The theory of the mechanical effects arising in the elastic cover was discussed by several groups. Refs. [1] and [2] investigates the role of the skin in the neural coding of primate tactile manipulation, while [3] and [4] analyzes the mechanical effects for utilization in future artificial tactile sensors. Nevertheless, precise experiments about the feasibility of the theoretical predictions on artificial sensors have not yet been reported.

In this paper we will check the validity and the limitations of the continuum-mechanical model [1], by providing experimental data, measured by a piezoresistive force-sensor array, capable of resolving all three vector components of the surface load. We also extend the capability of the sensors by applying various coatings, each with a different geometry. As a biological motivation, we try to mimic the function of the hairy skin and the fingerprints to enhance sensitivity to certain indentation types.

2. Sensor design

The sensor array (Fig. 1) is built up from monocrystalline-silicon sensory elements, all consisting of a central plate, suspended by four bridges over an etched cavity.

Each of the four bridges includes a p^+ piezoresistor that is used as an independent strain gauge. The two shear and one normal component of the surface load can be reconstructed from these four channels. The detailed description of the structure was recently reported [5].

The active sensory region was covered with silicon rubber[1] either by simply pouring the viscous material on the top, or by attaching a pre-made rubber layer with a well-defined thickness to the sensor, glued with some of the viscous material itself. In both methods, the elastomer forms a coating on the suspended membrane and infiltrates the cavity. In the former the thickness is purely controlled by the viscosity, while in the latter it can be chosen as preferred. Moreover, the latter method provides more freedom to form elastic coatings of various shapes.

3. Continuum mechanics

In order to characterize the covered sensor's performance, we need to calculate the stress and strain fields arising at the

* Corresponding author.
E-mail address: vasarhelyi@itk.ppke.hu (G. Vásárhelyi).

[1] Elastosil® RT-601.

0924-4247/$ – see front matter © 2006 Elsevier B.V. All rights reserved.
doi:10.1016/j.sna.2006.01.009

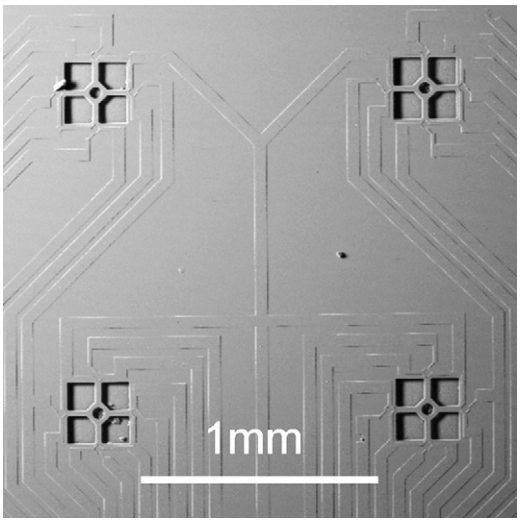

Fig. 1. Scanning-electron view of the 2 × 2 sensor array. All four sensory elements consist of a suspended cross-like bridge and four piezoresistors at the suspension points. Taxels (tactile pixels) are spaced 1.5 mm.

bottom of the elastic layer, as a result of the surface load. We will use the semi-infinite elastic model [6] and make the following assumptions: (1) the elastic material is linear, homogenous and treated as semi-infinite, (2) the rubber is incompressible—Poisson's ratio is 0.5, (3) the sensor measures the strain in the rubber, appearing at the center point of the piezoresistors.

First we analyze point loading. The equations below are derived from [6], and will be used as a theoretical reference for the strain distribution (Fig. 2(b)):

$$\begin{pmatrix} \gamma_x \\ \gamma_y \\ \varepsilon_z \end{pmatrix} = \frac{3(Qx + Fz)}{4\pi E(x^2 + y^2 + z^2)^{5/2}} \begin{pmatrix} 3xz \\ 3yz \\ x^2 + y^2 - 2z^2 \end{pmatrix} \quad (1)$$

where F is the normal, Q is one shear component of the load (the other is set to zero now for simplicity, reducing the 3D analysis to 2D), E the Young modulus, x, y and z are coordinates in the rubber (z points towards the sensor), γ_x, γ_y and ε_z are the two shear and one normal component of the strain tensor acting on the z plane.

4. Signal conditioning

An efficient and simple method is described in [7] for reconstructing the stress field at the sensor surface inside the rubber, by using the four bridge voltages. In contrast to the proposed method, we found that the deformation of the sensor bridges is a function of the strain field and not the stress. The structure of the equations, however, remains unchanged:

$$\gamma_x = \alpha_s(\Delta V_{left} - \Delta V_{right}), \qquad \gamma_y = \alpha_s(\Delta V_{down} - \Delta V_{up}),$$
$$\varepsilon_z = \frac{\alpha_n}{2}(\Delta V_{left} + \Delta V_{right} + \Delta V_{down} + \Delta V_{up}) \quad (2)$$

where γ_x, γ_y and ε_z are the strain tensor components, ΔV_i represents the measured voltage change, the α linear constants (shear and normal) contain the piezoresistive coefficients and all the information about the geometry of the sensor and the signal amplification.

5. Receptive-field measurements

In order to check the feasibility of the semi-infinite model, we carried out different experiments. First we measured the strain profile in the case of constant, normal loading. A sharp needle was slowly moved across the sensor surface along the x-axis (from left to right), and voltages were saved at 30 Hz. Measured strain components calculated with (2) are shown in Fig. 2(a), while theoretical components from (1) are shown in Fig. 2(b). In both cases Young modulus was set to 2.4 MPa, as calculated from the rubber's Shore A hardness of 45. Rubber thickness was 180 μm, total indentation force was 10 mN. Other measurement parameters are given in Table 1.

Lacking a detailed analysis of the geometry and the amplification factors, we arbitrarily choose 1/mV for the α_s and α_n constants. However, we are only interested now in the relative amplitudes of the strain components, so this simplification has no practical consequences.

To estimate the similarity of the two curves shown in Fig. 2, we measured some of their basic properties. For simplicity, we

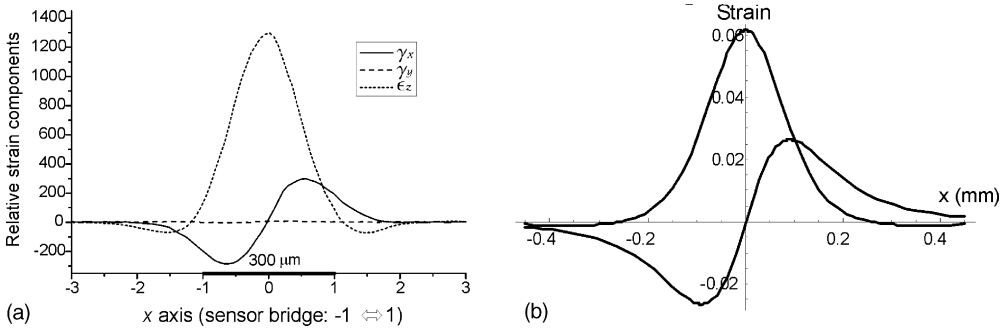

Fig. 2. Measured (a) and theoretical (b) strain components in the case of a point load, moving along the x-axis. On (a) the x-axis is scaled to the sensor size, the y-axis is presenting relative values only (as described in detail in the text). The general shape of the measured curves highly resembles that of the theoretical curves.

Table 1
Measurement conditions

Parameter	Value	Comment
PC	Pentium 4	With measurement software developed by us
A/D converter	Advantech PCI 1713	In the PC
Scanning frequency	30 Hz	Up to 50 Hz, higher values not needed yet
Voltage supply	5 V	For the sensor chip
Sensor sensitivity	4–6 mV/mN/V	Without cover and amplification
Sensor cover thickness	100–1000 μm	Less is too thin to work with, more is too thick to sense anything
Load range	0–10 mN	Maximum applicable load can be much higher, depending on cover thickness and indentation shape and size
Loading needle diameter	100 μm	Round shape
Amplification factor	50–60	Linear
Output range	1–1500 mV	After the amplification stage
Noise	2–3 mV	Mostly from the amplifier itself

analyzed the ε_z distribution. We used (1) to calculate the following:

$$\varepsilon_z = \max, \quad \text{where } x = 0, \qquad \varepsilon_z = \min, \quad \text{where } |x| = 2z,$$
$$\varepsilon_z = 0, \quad \text{where } |x| = \sqrt{2}z, \qquad \left|\frac{\varepsilon_{z\max}}{\varepsilon_{z\min}}\right| = 5^{5/2} \approx 56 \tag{3}$$

In the measurement shown in Fig. 2(a) $|\varepsilon_{z\max}/\varepsilon_{z\min}| \approx 19$, which indicates a much stronger lateral-inhibition effect than it is predicted. This is probably the result of the finite thickness, contrary to the infinite model.

In the second experiment we attached elastic layers of different thickness onto the same sensor, and compared the modified strain profiles (Fig. 3). We measured two features of the ε_z curve, i.e. the width and the amplitude, as functions of the rubber thickness at constant loading (Fig. 4). The two parameters vary according to the following equations (where rubber thickness is z):

$$W = 2\sqrt{2}z, \qquad A = \frac{3F}{2\pi E}\frac{1}{z^2} \tag{4}$$

where W is defined as the length between the two intersections of the curves and the x-axis, A is defined as the absolute maximum value of the ε_z curve at $x = 0$. Although the shape of the measurements resembles the theoretical curves, we are far from a perfect match. The measured W curve is linear, but its slope, 1.14 is different from the predicted 2.82. Also, the A curve can be fitted better with a $1/z^{1.45}$ function instead of the theoretical $1/z^2$. In other words, according to the measurements the ε_z curves are narrower than the prediction and their peak point declines less as rubber thickness grows. The difference in the characteristics of the curves is probably due to that in the geometry between the idealized theoretical and the real structure.

6. Inverse problem

As in many other fields of mathematics and physics, our final aim is to solve the "provoking" inverse problem, i.e. characterize the surface load by knowing only the strain measurements under the elastic cover. As usual, this could be done analytically only under very special circumstances. For example, assuming that we have a 2D point load at an arbitrary angle and position and we have three sensors at the same plane measuring the radial-stress components (which could be derived from the measured strain) at a defined position (Fig. 5), we could have three independent equations for three variables derived from the expressions for the radial-stress distribution [6]:

$$\sigma_{r_1} = \frac{-2}{\pi((x_2 - \mathrm{d}x)^2 + z^2)}(Pz + Q(x_2 - \mathrm{d}x)),$$
$$\sigma_{r_2} = \frac{-2}{\pi(x_2^2 + z^2)}(Pz + Qx_2),$$
$$\sigma_{r_3} = \frac{-2}{\pi((x_2 + \mathrm{d}x)^2 + z^2)}(Pz + Q(x_2 + \mathrm{d}x)) \tag{5}$$

As we can conclude, even in this very simplified, ideal case the solution for P, Q and x_2 is hard to find and measurement error can easily make solutions ambiguous. Nevertheless, we will see that there are different ways to overcome the inverse problem. First and foremost, we should keep it in mind that human mechanoreceptors under the skin deal with the same intriguing problem, and we are still able to use our hands to measure all surface properties of grabbed objects.

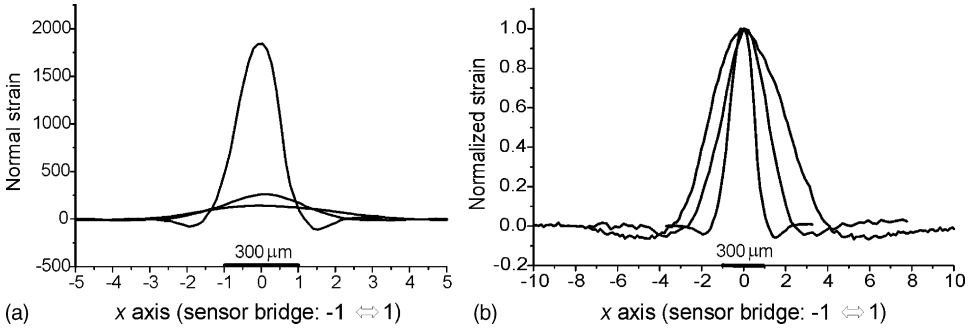

Fig. 3. (a) Measured strain at rubber thicknesses of 150, 580 and 850 μm. The width increases, the amplitude decreases with thickness. (b) The same curves normalized.

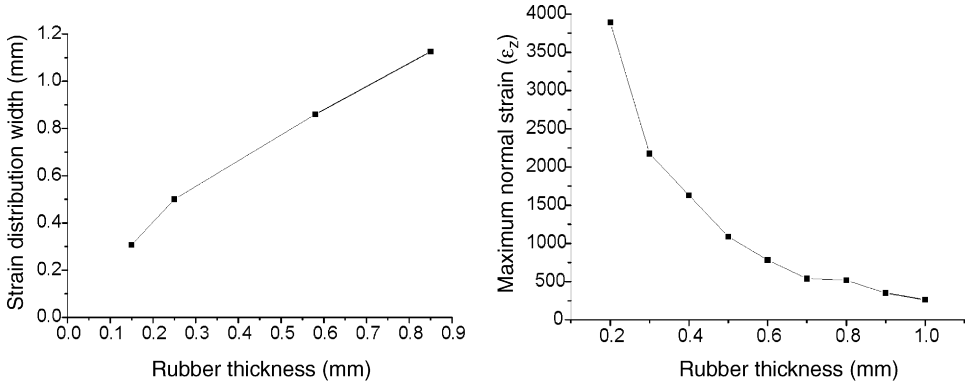

Fig. 4. As rubber thickness grows, the strain distribution flares and declines—the sensor looses sensitivity and acts more as a low pass filter.

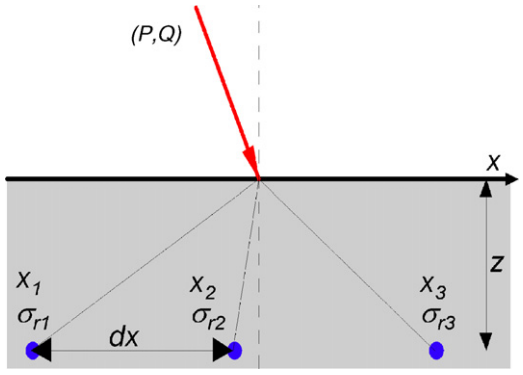

Fig. 5. The simplest model for the inverse problem. P and Q are two components of the load, σ_{r_i} is the measured radial-stress at the three sensors location (x_i), dx is sensor distance, z is the rubber thickness.

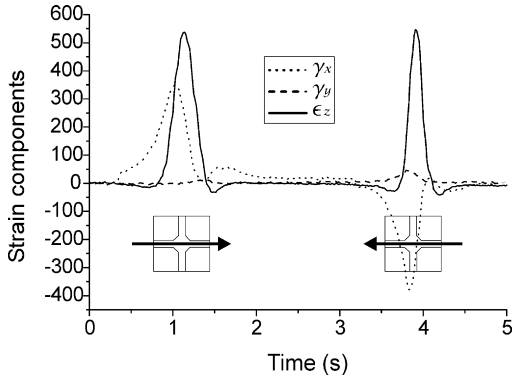

Fig. 6. Response of a hair-like sensor. Indentation moves from left to right and back along the x-axis, as depicted by the arrows below. ε_z is positive, one shear component is nearly zero, the other reflects motion direction.

There are two ways of mimicking nature in our case. First, we can treat the inverse problem as a direct one by taking only the useful information from the measurements, finding features that we can detect and training e.g. neural networks or any software to "understand" data. The success of this version depends on the software we design, which is analogous to the function of the brain in tactile perception. The other way is a hardware way. By introducing special elements to the sensor design, we can modify the sensor's receptive field and convert the complicated strain distribution into a more direct function of the surface load.

7. Hairy skin and shear sensitivity

From Fig. 2 it is clear that the shear sensitivity of our sensors is less than the prediction (the ratio of the maximum values of ε_z and γ_x is high). Shear sensitivity can be increased efficiently by attaching a rigid load-transmitting rod to the middle of the sensor membrane. This extra element acts the same way as a single hair in our skin—it elongates the force arm and sensitizes the structure to shear forces. Accordingly, the shape of the strain distribution changes fundamentally—lateral force components arising even at normal loading become dominant (Fig. 6). As friction pushes the rubber in the motion direction of the indentation, it evokes a greater response in the corresponding shear strain component. Therefore, indentation motion direction and the friction coefficient can be measured reliably by γ_x and γ_y, while indentation amplitude is still effectively marked by ε_z.

8. Fingerprints for sensitization

Fingerprints are often mentioned as personal identification clues but their real evolutional function is rarely known to the public. Papillary ridges are usually present on high-resolution tactile sensory systems (such as our fingers, some ape's tail, etc.)—they are known to serve as a mechanical amplification stage for stress transduction [8–10].

The emerging parts of any elastic cover enhance the stress transduction in two ways. First of all, if two materials contact, the location of the highest stress values is always around the first contact points. Secondly, due to the complex behavior of the elastic material, some components of the stress and strain distribution reach their peak value right below the highest and lowest points of a modulated surface [8]. As an indirect proof, we find the human mechanoreceptors located at these points, respectively (Fig. 7) [10].

In order to measure the effect of different types of undulations on the elastic cover, we investigated two basic types of rough surfaces: one with simple semi-spherical bumps formed above each sensor, one with fingerprint-like ridges (Fig. 8). Both types are moulded together with the normal elastic cover. The negative

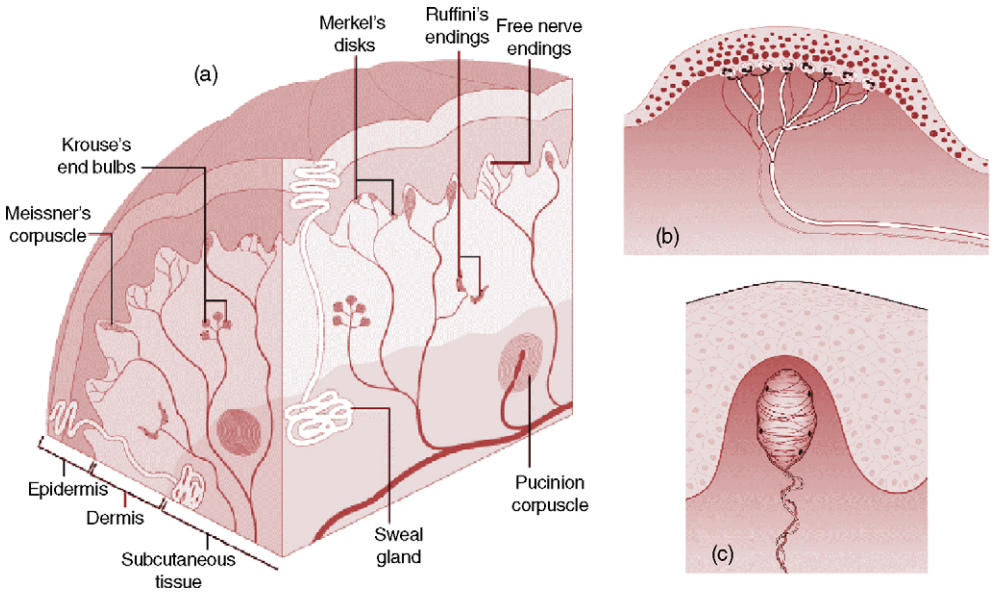

Fig. 7. (a) Schematic cross-section of the human skin. Merkel and Meissner mechanoreceptors are located at the junction of the dermis and the epidermis, under the papillary ridges. (b) Enlarged view of a Merkel receptor dome. (c) Schematic view of a Meissner receptor complex (All images are from http://www.ilo.org/encyclopaedia/).

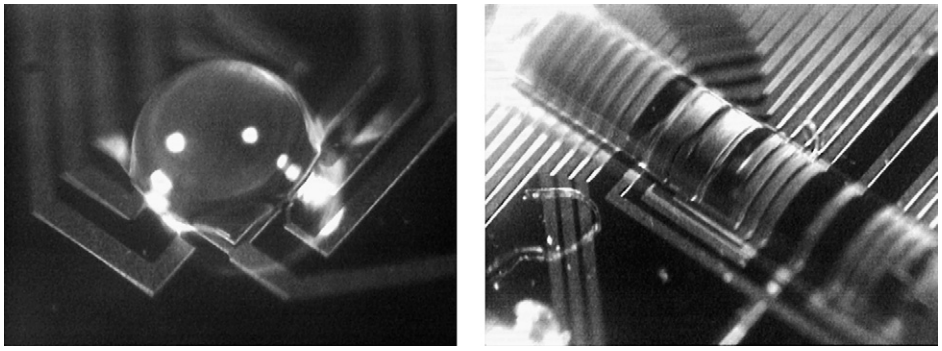

Fig. 8. Microscopic view of different elastic bumps formed on the sensor surface to mimic fingerprints and enhance stress/strain transduction.

mould is made from a simple silicon wafer by homogeneous etching. The elastic layer is around 200 μm thick, the bump and the ridge is 250–280 μm high. We varied the diameter of the bump and the width of the ridge between 360 and 760 μm to find the optimal size.

The new geometry of the cover changes the receptive field of the sensors in two ways. Besides sensitizing the structure as described above, it changes the response shape of the sensors at indentation. For analyzing the new properties we carried out two experiments.

As a first quantitative measurement we used the cover with simple spherical bumps. We attached the covering layer to two identical sensors in a way that one sensor had a bump above it and the other did not. Then our finger (as an arbitrary load) was moved around many times concentrically over the sensors. This experiment is rather a real tactile scene than a precise measurement, but results in Fig. 9 clearly prove that sensors with elastic bumps on top have increased lateral sensitivity, they react more vigorously to arbitrary forces.

For precise testing we used a simple screw, moved over the sensors laterally, creating a series of point loads. We compared the shape of the measured strain distributions in four cases: (1) sensor with a flat elastic surface, (2) sensor with a spherical bump on top, (3) sensor with a ridge, indentation moving parallel with the ridge, (4) same sensor, but with indentation motion perpendicular to ridge orientation. Results can be seen in Fig. 10.

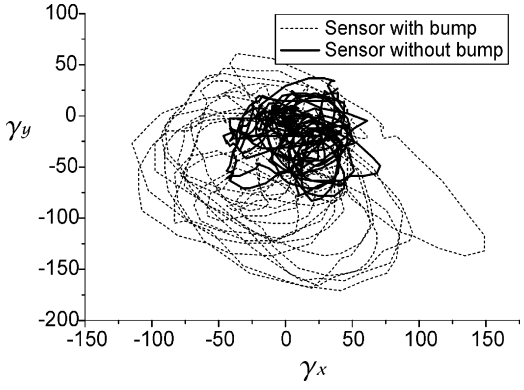

Fig. 9. Response of two identical sensors, one with an extra bump on top of the elastic layer. The two axes are the two tangential strain components—curves thereby correspond to the lateral finger motion over the sensors. Sensitivity is increased by the elastic fingerprint-like bump.

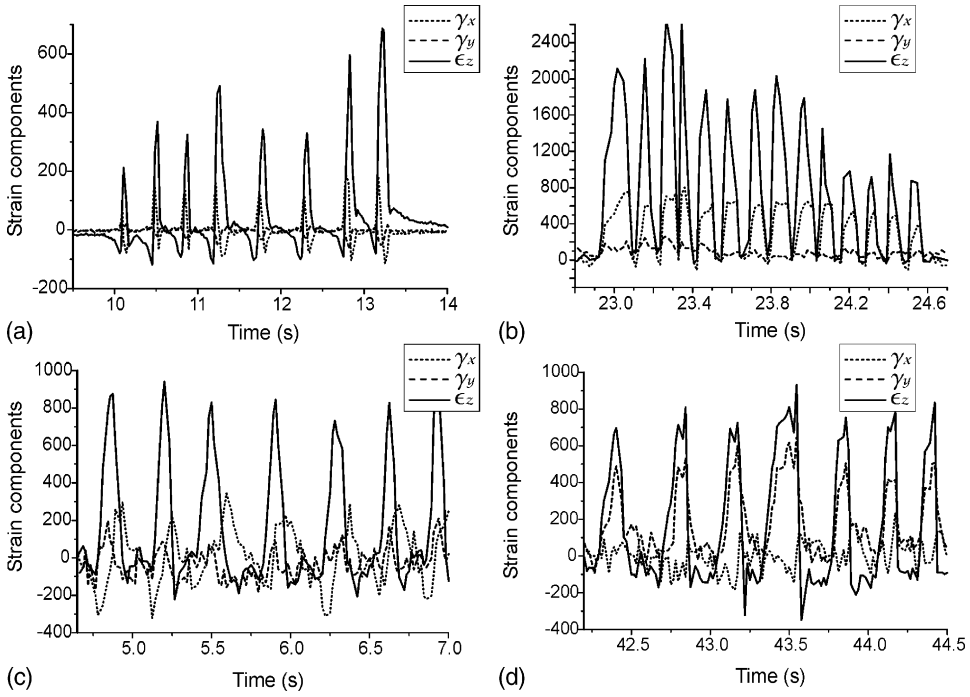

Fig. 10. Response of different sensors to a series of point loads, moving over the sensors in time. (a) Elastic cover with flat surface; (b) elastic bump over the sensor; (c) fingerprint-like ridge over the sensor, indentation motion parallel with the ridge; (d) same sensor but indentation motion perpendicular to the ridge.

Fig. 10 illustrates that either a bump or a ridge perpendicular to the indentation motion changes the original point-load characteristics into a more direct function of the surface load. The bump (Fig. 10(b)) and the ridge (Fig. 10(d)) integrate the load from their entire surface and respond to the amplitude of the load and the shear force direction, which corresponds to the indentation–motion direction. The flat surface (Fig. 10(a)) and the ridge parallel to indentation–motion direction (Fig. 10(c)) represent the complicated strain distribution, as described by the semi-infinite model.

We can conclude that besides enhancing the sensitivity, the modified geometries are efficiently and directly coding different properties of the indentation. Moreover, we could demonstrate the direction selectivity of the fingerprint-like ridges, which could also be used to prove the direction selectivity of human mechanoreceptors under real fingerprints.

9. Conclusions

The semi-infinite enables us to describe the properties of tactile sensor's coverage—although unlike in [8], the measured profiles match the strain distribution better than the stress. The measured and calculated shapes look similar, therefore, we can use the model to forecast the sensor's final properties. The proper cover design can be chosen to have best receptive field size at the expense of sensitivity.

Compared to the theoretical model, the measured distributions are narrower and reflect a stronger lateral-inhibition property. The latter might be a useful side effect, when the receptive fields in a sensor array are overlapping. In this case it can enhance the lateral spatial resolution of the sensor (which is the case in biological systems, too).

The inverse problem of the flat elastic cover is hard to find, instead we can change to geometry of the sensor cover to represent different properties of the indentation more directly. To achieve this, we mimic human tactile perception and introduce hair- and fingerprint-like elements to the sensor design. This way we could enhance the sensor's sensitivity to different indentation types and features without reducing the level of protection. These additions are proved to be efficient in the sensor technology, and could be used for extending our knowledge on our own tactile system, too.

Acknowledgments

Special thanks are due to our technician, Attila Nagy, who insistently assembled all the unique sensors we needed. Part of this work was supported by the Hungarian Scientific Research Found (OTKA) via grant no. T47002.

References

[1] J.R. Phillips, K.O. Johnson, Tactile spatial resolution. III. A continuum mechanics model of skin predicting mechanoreceptor responses to bars, edges, and gratings, J. Neurophysiol. 46 (6) (1981) 1204–1225.
[2] K. Dandekar, B.I. Raju, M.A. Srinivasan, 3D finite-element models of human and monkey fingertips to investigate the mechanics of tactile sense, J. Biomech. Eng. 125 (5) (2003) 682–691.
[3] M. Shimojo, Mechanical filtering effect of elastic cover for tactile sensor, IEEE Trans. Robotics Automat. 13 (1) (1997) 128–132.
[4] R.S. Fearing, Tactile sensing mechanisms, Int. J. Robotics Res. 9 (3) (1990) 3–23.
[5] M. Ádám, É. Vázsonyi, I. Bársony, G. Vásárhelyi, Cs. Dücső, Three dimensional single crystalline force sensor by porous Si micromachining, in: Proceedings of IEEE Sensors, Vienna, 2004.
[6] K.L. Johnson, Contact Mechanics, Cambridge University Press, 1985.

[7] B.J. Kane, M.R. Cutkosky, G.T.A. Kovacs, A traction stress sensor array for use in high-resolution robotic tactile imaging, J. Microelectromech. Syst. 9 (4) (2000) 425–434.
[8] R.S. Fearing, J.M. Hollerbach, Basic solid mechanics for tactile sensing, Int. J. Robotics Res. 4 (3) (1985).
[9] G.J. Gerling, G.W. Thomas, The Effect of Fingertip Microstructures on Tactile Edge Perception, WHC, 2005, pp. 63–72.
[10] D. Yamada, T. Maeno, Y. Yamada, Artificial finger skin having ridges and distributed tactile sensors used for grasp force control, J. Robotics Mech. 14 (2) (2002) 140–146.

Biographies

Gábor Vásárhelyi was born in Budapest, Hungary, in 1979. He received his MSc degree in engineering-physics from the Technical University of Budapest, Hungary, in 2003. He is currently a PhD student at Péter Pázmány Catholic University, Multidisciplinary Technical Sciences Doctoral School, Budapest, Hungary. Main research fields are tactile sensor arrays and tactile applications on CNN chips.

Mária Ádám was born in Hungary, in 1948. She received the MSc degree in electrical engineering from the Technical University of Budapest, Hungary, in 1973. She was R&D Engineer at TUNGSRAM Ltd., at the Department of Semiconductors, from 1973 to 1982. From 1982 to 1985 she spent 3 years with the Microelectronics Co. Currently, she is research engineer at the MEMS Laboratory of the Research Institute for Technical Physics and Materials Science (MFA). Her research interests include design, development and processing of silicon-based mechanical and gas-microsensor structures. She is co-author of about 25 scientific papers and one patent.

Éva Vázsonyi was born in Hungary, in 1941. She received her MSc degree in chemical engineering from the Technical University of Budapest, Hungary, in 1965. She worked for the TUNGSRAM Ltd. at the Department of Semiconductors and later joined the Technical University as a research fellow. In 1972, she joined the Central Research Institute for Physics and currently she works for one of its successor, the MEMS Laboratory MFA. Her research interests include fine line lithography and silicon micromachining. She has four patents and author and co-author of about 60 scientific papers.

István Bársony was born in Hungary, in 1949. He graduated in electrical engineering and holds PhD and DSc degrees in microelectronics. At present he is director of MFA, Budapest and professor of nanotechnology at the University of Veszprém, Hungary. His research interests are Si microtechnology, MEMS and nanotechnology. He authored and co-authored over 100 scientific papers and holds 13 patents.

Csaba Dücső was born in Hungary, in 1959. He graduated as a chemist in 1983 and received the PhD degree in chemistry from the Lóránd Eötvös University, Budapest, Hungary. Currently, he is head of the MEMS laboratory of MFA, Budapest. His research interests include Si-based MEMS, with special emphasis on integrated gas and mechanical sensors and the development of the related processing technology. He is co-author of over 50 papers published in periodicals and conference proceedings.